AIP Advances

Core–shell behavior and exchange bias of Fe-doped CuO nanoparticles

Cite as: AIP Advances **10**, 065009 (2020); https://doi.org/10.1063/5.0008366
Submitted: 23 March 2020 . Accepted: 12 May 2020 . Published Online: 02 June 2020

Aline Alves Oliveira, Marlon Ivan Valerio-Cuadros, Alex Soares de Brito, Lilian Felipe Silva Tupan, Flávio Francisco Ivashita, Julian Geshev, and Andrea Paesano

Core–shell behavior and exchange bias of Fe-doped CuO nanoparticles

Cite as: AIP Advances 10, 065009 (2020); doi: 10.1063/5.0008366
Submitted: 23 March 2020 • Accepted: 12 May 2020 •
Published Online: 2 June 2020

Aline Alves Oliveira,[1] Marlon Ivan Valerio-Cuadros,[1] Alex Soares de Brito,[1] Lilian Felipe Silva Tupan,[1] Flávio Francisco Ivashita,[1] Julian Geshev,[2] and Andrea Paesano, Jr.[1,a)]

AFFILIATIONS

[1] Departamento de Física, Universidade Estadual de Maringá, Av. Colombo 5790 - Jardim Universitário, 87020-900 Maringá, PR, Brazil

[2] Instituto de Física, UFRGS, Porto Alegre 91501-970 Rio Grande do Sul, Brazil

[a)] **Author to whom correspondence should be addressed:** paesano@wnet.com.br. **Tel.:** +554430115928

ABSTRACT

$Cu_{1-x}Fe_xO$ nanoparticles were prepared using a freeze-drying process followed by heat treatment. The particles were then characterized using Mössbauer spectroscopy and magnetization techniques. The results revealed complex magnetic behavior, which can be attributed to the presence of two different magnetic regions: the particle core, which has antiferromagnetic fluctuations, and the particle shell, where uncompensated spins are responsible for their superparamagnetic characteristics. At low temperatures, the moments freeze, revealing a ferromagnetic order for the shells and a dipolar magnetic interaction among the nanoparticles. In addition, an exchange-bias field revealed magnetic interactions between the core and the shell of the nanoparticles. The ferromagnetism observed in this system suggests that antiferromagnetic oxide matrices can be used for diluted magnetic semiconductor applications, if suitably doped.

I. INTRODUCTION

Materials that could transport a spin-polarized electric current have attracted much attention in recent decades. The interest has been triggered by theoretical models that predicted that a nonmagnetic oxide matrix doped with magnetic cations should present a ferromagnetic (FM) order at room temperature (RT).[1,2] Such materials are called diluted magnetic oxides (DMOs), which have been prepared through several combinations of hosts (e.g., III-V semiconductors) and magnetic cations (e.g., Mn, Co, and Fe).[2] The structures and magnetic states of DMOs have been extensively characterized. While preserving their semiconductor properties, these oxides could solve the lack of semiconductors that are typically FM at RT.

However, there is hardly any definitive data on the true FM nature of DMOs due to problems related to the presence of minor phases and doubtful magnetic characterization. The absence of conclusive results is partly due to the possible formation of minor (magnetic) phases during DMO synthesis. These spurious phases are difficult to identify and could mask the true (non-)magnetic nature of the prepared solid solutions. In addition, a real DMO is supposed to present weak FM yields, which cannot be confounded with magnetization measurement artifacts.[2] Therefore, well-performed phase identification and accurate magnetization measurements are essential to clarify the true phasic and magnetic characteristics of the doped oxides. Some promising DMO candidates are only FM at low temperatures, making them unsuitable for RT applications and demanding further investigation.

One possible strategy to prepare oxide semiconductors that are FM at RT could be doping with magnetic cation nanoparticles, which are antiferromagnetic (AFM) oxides in the bulk state. The FM behavior has already been observed in undoped oxide nanoparticles and attributed to uncompensated spins at the surface nanoparticles. Doping these nanoparticles with magnetic cations, particularly, those with a larger magnetic moment, could enhance the nanoparticle FM moment and make them appropriate for spintronic applications. In other words, the FM fraction of the system could transport a spin polarized current.[3,4]

Focusing on this possibility, we synthesized Fe-doped CuO nanoparticles by lyophilization followed by heat treatment. We

recently reported some of the structural and optical properties of the nanoparticles.[5] These nanostructures were shown to be effectively monophasic by high-resolution XRD, and a correlation was also established between the dopant concentration and particle size.

CuO is a p-type semiconductor that has a narrow band gap (1.2–1.4 eV) and two AFM transitions near 215 K and 230 K.[6] Many studies on CuO doped with transition metal (TM = Mn, Fe, Co, and Ni) have been conducted due to the sharp changes in several physical properties that doping induces. The modifications include optical, electric, and magnetic properties that depend on the dopant and the synthesis route of the nanostructures.[7–13] Most of the time, it has been observed that doping reduces the size of the particles to the nanometer scale, giving rise to complex magnetic properties such as antiferromagnetism coexisting with ferromagnetism or superparamagnetism, uncompensated surface spins in antiferromagnetic nanoparticles, exchange bias, and spin glass.

Some studies have been conducted on CuO doped with Fe cations, which usually assume a trivalent state when diluted in oxides and, hence, have a magnetic moment of pure spin. For example, Manna and De[14] prepared Fe-doped CuO nanorods using a hydrothermal method and reported feeble ferromagnetism at RT. The nanoparticle shape anisotropy was found to determine the magnetic behavior of the $Cu_{1-x}Fe_xO$ nanorods, and ferromagnetism was considerably enhanced by the substitution of iron in the copper sites. Gaur *et al.*[15] reported the synthesis of Fe-doped CuO nanostructures using a wet chemical method. They observed superparamagnetic (SPM) behavior at RT, and the blocking temperature decreased as the particle size decreased. In addition, all the samples exhibited FM behavior at T = 5 K, and the magnetic order was shown to increase as the iron concentration increased.

One great advantage of the Fe-doping of oxides is the possibility of applying Mössbauer spectroscopy, which can finely identify minor phases and different iron sites in the analyzed sample, as shown by others.[11,16] This was our main reason for using Fe as a dopant. Preliminary Mössbauer spectroscopy and magnetization analysis results were also, recently, reported for $Cu_{1-x}Fe_xO$ samples (i.e., x = 0.01 and 0.03).[17] The magnetic behavior of the $Cu_{1-x}Fe_xO$ nanoparticles is complex. Macroscopic magnetic analysis revealed SPM particles at RT, while hyperfine interactions on the ^{57}Fe indicated the presence of two magnetic phases. We suggested that one of these phases could correspond to a nanoparticle region characterized by AFM fluctuations. The other phase would correspond to a region where uncompensated spins are responsible for the SPM characteristics and ultimately the FM interactions among the nanoparticles at low temperatures (LT).

The FM interactions that occur near RT make this system promising as a DMO and worthy of further investigation. Therefore, we studied new doping concentrations to better understand the magnetic properties of the $Cu_{1-x}Fe_xO$ nanoparticles and give a more general and conclusive description for this system. $Cu_{0.98}Fe_{0.02}O$ and $Cu_{0.96}Fe_{0.04}O$ nanoparticles were prepared and characterized by magnetization vs temperature [$M(T)$] curves and Mössbauer spectroscopy from RT down to 4.2 K. The magnetization vs magnetic field [$M(H)$] curves were also applied in the search for evidence of exchange bias (EB).

In this paper, we corroborate the presence of two magnetic phases that share the same interface and are magnetically coupled. Furthermore, we propose a model to structurally and magnetically describe the $Cu_{1-x}Fe_xO$ nanoparticles. The results are key information for tuning the doping synthesis of this semiconductor oxide and could have technological applications in spintronics.

II. MATERIAL AND METHODS

$Cu_{1-x}Fe_xO$ nanoparticles were prepared by freeze-drying an aqueous solution of copper acetate and ^{57}Fe acetates, followed by heat treatment, as detailed in Ref. 5. The structure and phase purity were checked by high resolution x-ray powder diffraction and the estimated crystallite sizes for $x = 0.02$ and 0.04 were 25 nm and 16 nm, respectively.[5] The magnetic properties were performed using a vibration sample magnetometer (Quantum Design MPMS-3 SQUID-VSM). The zero-field cooling (ZFC) and field cooling (FC) magnetization curves $M(T)$ were measured at 250 Oe for both samples and (ZFC) and field cooling magnetization curves $M_{ZFC}(T)$ at different magnetic applied field values (10, 50, 150 and 250 Oe) only for x = 0.04. The $M(H)$ curves were taken at 5 K, 10 K, 100 K, and 300 K for 70 kOe ≤ H ≤ 70 kOe for both ZFC or FC protocols. Mössbauer spectroscopy was performed in transmission geometry using a ^{57}Co(Rh) source with 50 mCi of nominal activity. A metallic iron foil absorber (α-Fe) was used to calibrate the velocity scale. The spectra were obtained at 300 K, 200 K, 150 K, 100 K, 50 K, 25 K, and 4.2 K using a closed-cycle He cryostat.

III. RESULTS

A. Magnetic and morphological characterization

The $M(T)$ curves for the $Cu_{0.98}Fe_{0.02}O$ and $Cu_{0.96}Fe_{0.04}O$ samples are shown in Figs. 1(a) and 1(b), respectively. These ZFC/FC curves are very similar to those simulated for a system that contains a SPM phase with log–normal distribution of the particle size;[18] they also are analogous to our experimental results for the $Cu_{0.97}Fe_{0.03}O$ sample.[17] Thus, the ZFC/FC curves suggest a behavior consistent with a system of SPM particles at RT that become FM at the lowest temperatures.

The ZFC peak occurs at different temperatures for the two samples (133 K for $x = 0.02$ K and 140 K for $x = 0.04$). This particular temperature corresponds to the blocking temperature, T_B, below which the particle moments are frozen, i.e., ferromagnetic ordering in the time scale of the measurement.[19] The broadening of the ZFC peak reveals a distribution for the crystallite size, which is consistent with our observations on the particle morphology of this system [see Fig. 1(c)]. T_B varies depending on the applied magnetic field value as shown in Fig. 1(d) for the $Cu_{0.96}Fe_{0.04}O$ sample; the value of T_B is shifted toward higher temperatures with increasing H. The nature of the possible inter-particle interaction can be assessed from the field dependence of T_B.[20] Figure 1(d) shows the variation of T_B as a function of $H^{2/3}$, which is a typical Almeida-Thouless line, suggesting a dipolar interaction between the nanoparticles.[20] We will return to this subject later.

Figure 2 presents $M(H)$ curves for the $Cu_{0.98}Fe_{0.02}O$ and $Cu_{0.96}Fe_{0.04}O$ nanoparticles, traced at 10 K and 300 K. Each of these $M(H)$ curves, which are not saturated up to H = 70 kOe, can be

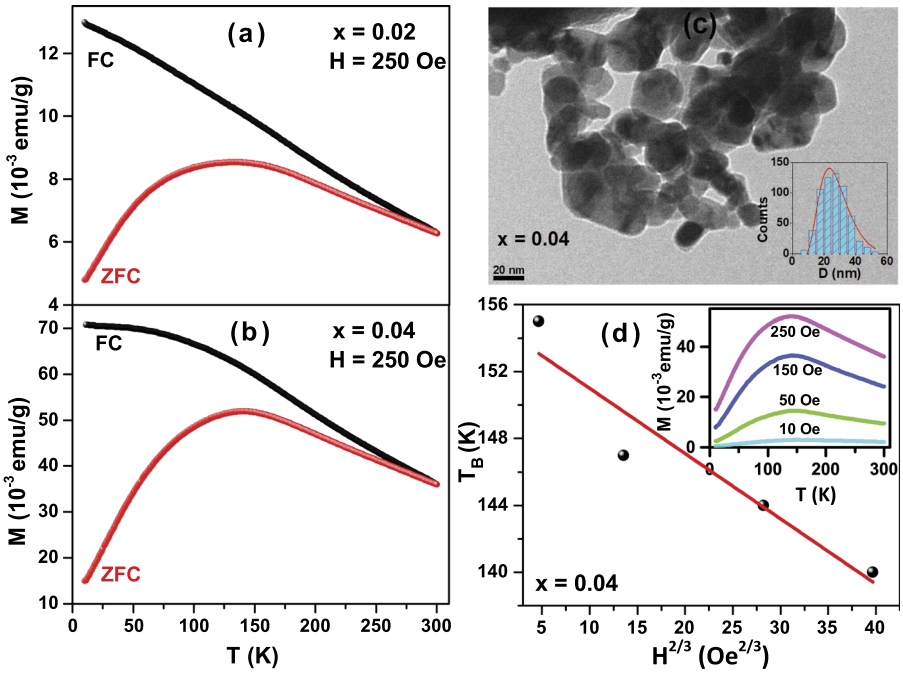

FIG. 1. Magnetization vs temperature curves for the $Cu_{0.98}Fe_{0.02}O$ (a) and $Cu_{0.96}Fe_{0.04}O$ (b) samples; TEM micrograph and histogram (inset) of the particle size taken from the $Cu_{0.96}Fe_{0.04}O$ sample (c); T_B as a function of $H^{2/3}$ and $M_{ZFC}(T)$ curves measured for different magnetic fields (inset) for the $Cu_{0.96}Fe_{0.04}O$ sample (d).

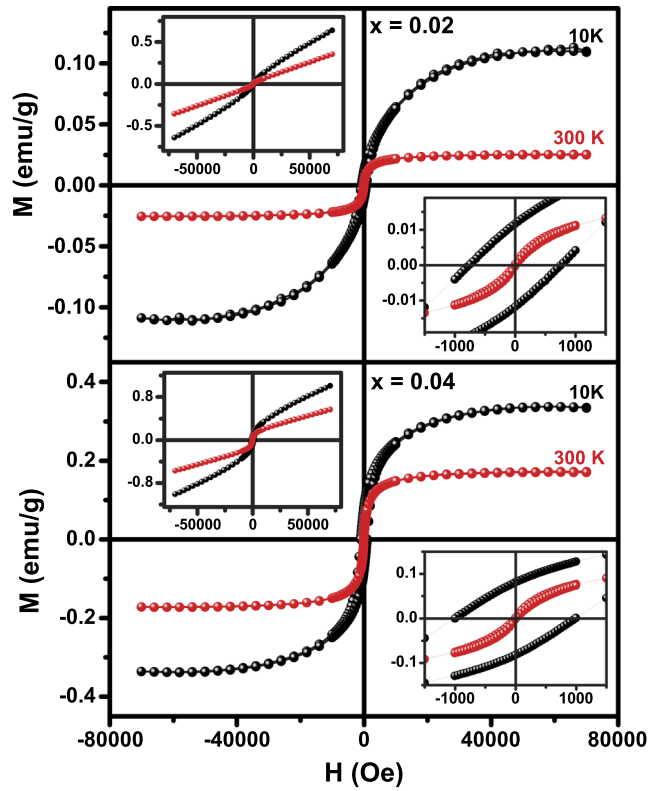

FIG. 2. $M_{FM}(H)$ curves for the $Cu_{0.98}Fe_{0.02}O$ and $Cu_{0.96}Fe_{0.04}O$ samples measured at 10 K and 300 K; the insets on the right show a zoomed-in image of the respective low-field range; each inset on the left shows the complete $M(H)$ curve.

interpreted as a sum of two contributions and may consistently be represented as $M(H) = M_{FM}(H) + \chi_{AFM} H$. The first term accounts for a hysteretic component, and the second term refers to a linear component of the magnetization (i.e., χ_{AFM} is the susceptibility of the AFM phase), as considered for the $x = 0.01$ and 0.03 samples.[17] Such a system is expected to be a Langevin paramagnet above T_B and exhibiting magnetic hysteresis below T_B. This behavior is clearly observed for both samples, evidencing the SPM character of nanoparticles for $T > T_B$ and the FM blocked state for $T < T_B$.

These curves revealed the saturation magnetizations (M_S), coercive fields (H_C), and remnant magnetization (M_R) values, which are listed in Table I. All these increase with iron concentration and decrease with T. In addition, χ_{AFM} increases with the iron concentration and decreases with T. These results also confirm the dual character, FM and AFM, of the samples at low temperatures.

B. Mössbauer analysis

The Mössbauer spectra obtained for the $Cu_{0.98}Fe_{0.02}O$ and $Cu_{0.96}Fe_{0.04}O$ samples at RT and below are shown in Fig. 3. They are comparable to those obtained earlier for $Cu_{0.99}Fe_{0.01}O$ and $Cu_{0.97}Fe_{0.03}O$ and were equally fitted with a discrete sextet and a hyperfine magnetic field distribution (B_{hf} Dist.).[17] The hyperfine parameters and sub-spectral areas are listed in Table II.

The hyperfine parameters and their variation with the temperature are very similar for both samples. For the two spectral contributions, the isomer shifts (δ) have similar values and are typical of Fe^{3+}. They increase when the temperature drops due to the second-order Doppler effect. The quadrupole splitting (2ε) obtained for the

TABLE I. Magnetic parameters for the $Cu_{1-x}Fe_xO$ samples.

Sample (x)	H_C (Oe)		M_R (10^{-3}emu/g)		M_S (10^{-3}emu/g)		X (10^{-6}emu/g.Oe)	
	10 K	300 K	10 K	300 K	10 K	300 K	10 K	300 K
0.02	761	14	12	0.3	115	25	7.6	4.7
0.04	995	17	82	2.2	344	172	9.6	5.7

distribution are small or almost null and are relatively temperature-independent. As expected for B_{hf} distributions, the fitted 2ε parameter represents an average over values, which, in this case, may be as high as 1 mm/s (e.g., when $B_{hf} \approx 0$).

Regarding the strength of the magnetic interactions, their evolution with the temperature is more complex. For both samples, the hyperfine field distribution exhibited an increase in the average value of B_{hf} as a result of the temperature reduction (see Fig. 3). This behavior has been observed in Mössbauer spectra of iron-doped CuO samples by other authors,[11,16,21] and is typical of progressive magnetic phase ordering. Here, the AFM order is expected to occur due to similarity with the known behavior of undoped CuO. On the other hand, the discrete sextet maintains the same B_{hf} value for different temperatures (see Fig. 4), while Γ decreases with decreasing temperature. This spectral evolution with the temperature is the hyperfine signature of SPM relaxation,[22] in agreement with the M vs T results.

In the case of ^{57}Fe Mössbauer spectroscopy, below T_B, the Mössbauer spectra should present a six-line (one sextet) component for each magnetic iron site in the material. For temperatures above T_B, the iron atomic moment fluctuates so fast (i.e., with a relaxation time that is short compared with the Mössbauer probing timescale) that the nucleus sees a null average B_{hf}, i.e., the spectra would consist of singlets or doublets. Complex spectra may result for medium relaxation times, and fits with appropriate mathematical routines must be applied.[23,24] In the present case, the relaxation time is longer than the Mössbauer spectroscopy time window, and, thus, the spectra consist of sextets with lines that become increasingly sharper as the temperature decreases.

The relative areas of the two main spectral contributions remained nearly constant at different temperatures. In Ref. 17 we suggested that this behavior indicates a two-phase spin system, which progresses more or less independently as the temperature drops.

IV. DISCUSSION

Considering all the previous results obtained, including the morphology of the nanoparticles, it is plausible to attribute the two

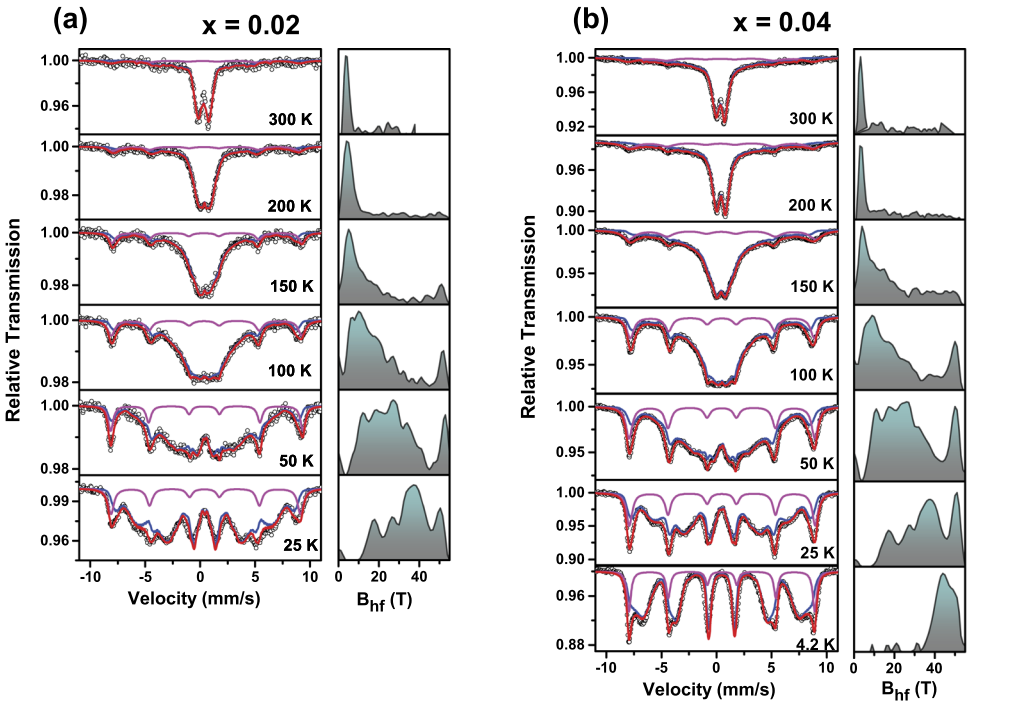

FIG. 3. Mössbauer spectra taken at different temperatures for the $Cu_{0.98}Fe_{0.02}O$ (a) and $Cu_{0.96}Fe_{0.04}O$ (b) samples. The respective hyperfine magnetic field distributions are shown at the right of the spectra.

TABLE II. Hyperfine parameters and sub-spectral areas for the $Cu_{1-x}Fe_xO$ samples.

Sample (x)	T (K)	Site	δ[a] (mm/s)	2ε (mm/s)	B_{hf}[b] (T)	Γ (mm/s)	Area (%)
0.02	300	B_{hf} Dist.	0.31	−0.02	10.0	0.27	85
		Sextet	0.34	0.26	53.0	1.41	15
	200	B_{hf} Dist.	0.40	−0.01	12.2	0.27	86
		Sextet	0.43	0.31	53.0	1.10	14
	150	B_{hf} Dist.	0.43	0.05	16.2	0.27	85
		Sextet	0.49	0.30	53.7	0.74	15
	100	B_{hf} Dist.	0.45	0.01	19.4	0.27	83
		Sextet	0.47	0.23	53.8	0.79	17
	50	B_{hf} Dist.	0.45	−0.02	27.0	0.27	85
		Sextet	0.50	0.23	54.3	0.54	15
	25	B_{hf} Dist.	0.43	0.03	34.1	0.27	85
		Sextet	0.50	0.12	53.5	0.65	15
0.04	300	B_{hf} Dist.	0.35	−0.03	13.3	0.27	80
		Sextet	0.34	0.06	51.9	1.80	20
	200	B_{hf} Dist.	0.40	−0.02	14.3	0.27	79
		Sextet	0.40	0.11	51.9	1.56	21
	150	B_{hf} Dist.	0.41	0.01	17.8	0.27	80
		Sextet	0.47	0.10	52.6	1.40	20
	100	B_{hf} Dist.	0.41	−0.04	20.9	0.27	80
		Sextet	0.50	0.05	51.8	0.80	20
	50	B_{hf} Dist.	0.42	−0.04	27.0	0.27	79
		Sextet	0.48	0.02	52.3	0.69	21
	25	B_{hf} Dist.	0.44	−0.05	35.1	0.27	80
		Sextet	0.50	0.05	52.3	0.62	20
	4.2	B_{hf} Dist.	0.44	−0.05	44.6	0.27	78
		Sextet	0.49	−0.03	52.3	0.46	22

[a]Relative to α-Fe measured at RT.
[b]B_{hf} average, in case of hyperfine magnetic field distribution.

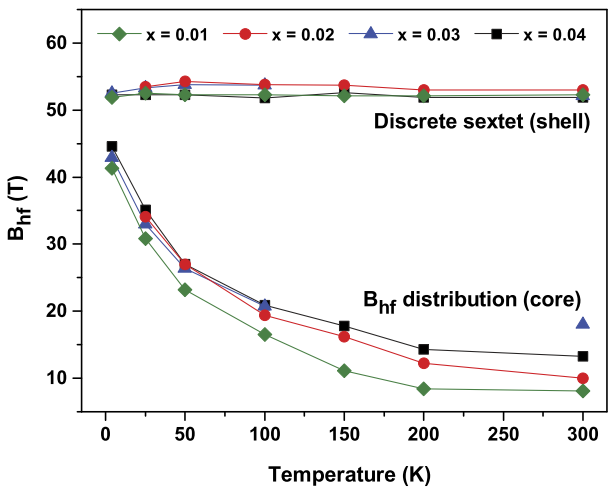

FIG. 4. B_{hf} of the discrete sextets and B_{hf} average of the distributions as a function of temperature for both samples. Data for $x = 0.01$ and $x = 0.03$ are compiled from Ref. 17.

different magnetic phases to two different regions in the nanoparticles: the core and the shell (Fig. 5).

The former is an AFM nanophase, which orders progressively under reducing temperature. The latter is a surface layer with uncompensated spins and, therefore, with a net magnetic moment that fluctuates with a rate that is dependent on temperature. It is a SPM nanophase above T_B, and the spins are blocked below T_B. This core–shell model is consistent with all the experimental data obtained in this investigation.

In fact, a similar description was proposed before by Néel in 1961 for materials structured in nanoscale, which are AFM in bulk dimensions. Within the original Néel model, reducing the size of the AFM particles to the nanoscale dimension, two sublattices are present: an internal perfect structured (core) and a defected surface with spin imbalance (shell). When the surface-to-volume ratio becomes sufficiently large, the uncompensated spins at the surface can yield a detectable net magnetic moment, exhibiting superparamagnetism and weak ferromagnetism.

A pertinent question is whether the thickness of the SPM surface layer varies with the iron concentration doping or does it remain constant. An estimate using the subspectral Mössbauer areas—which represent the relative volume of the phases—supposing (i) spherical shaped nanoparticles and (ii) that the nanoparticles are homogeneously doped, is shown in Table III. The results, including samples previously characterized, show that the shell thickness is approximately constant, i.e., it does not depend on x.

The presence of two magnetic phases in contact raised the possibility of manifestation of EB in these nanoparticles, which was further studied via $M(H)$ curves measured for both FC and ZFC protocols. Figure 6 shows the $M(H)$ taken below and above T_B for both samples. A shift in the hysteresis loop along the field axis is observed when each of the systems is cooled down in an external magnetic field through the Néel temperature of the AFM region (i.e., the core). Table IV shows the EB parameters extracted from the curves of Fig. 6.

The major magnetization hysteresis loops traced at 10 K for both $x = 0.02$ and 0.04 are not saturated, i.e., the magnetization reversal at the high-field regions is not reversible. It is usual for highly anisotropic magnetic systems to show minor-loop effects if the maximum measurement field, H_{max}, is not sufficiently strong for effective saturation along one of the branches of the hysteresis cycle, which might lead to possible incorrect interpretations of the observed field shifts.[25] Thus, we surmise that each of the H_{EB} values measured at 10 K and given in Table IV most likely represents a sum of the EB field and a field shift due to minor-loop effects. We checked whether the $M(H)$ loops measured at 100 K after FC are saturated by applying one of the criteria for discriminating non-saturated (minor) from saturated (major) hysteresis loops.[25] Both the first and the second derivatives of the ascending and descending branches of each major loop traced at 100 K (Figure S1 of the supplementary material) coincide for $|H| \geq 10$ kOe, i.e., for fields much lower than our $H_{max} = 70$ kOe. Therefore, the 100 K field-shift values given in Table IV only represent EB fields. The observation of EB offers strong evidence for the existence of two magnetic phases in these samples.

As mentioned before, the correlation between T_B and H might indicate interparticle interactions. To elucidate this question,

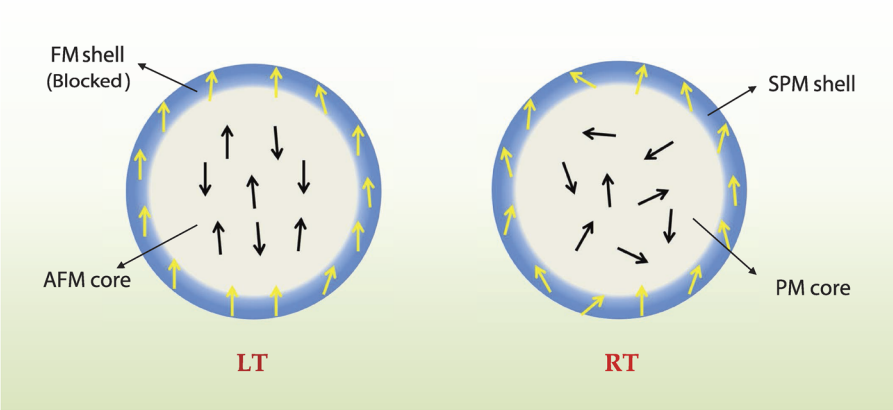

FIG. 5. The magnetic state of a core–shell nanoparticle at low and room temperatures.

TABLE III. Particle, core, and shell sizes of the $Cu_{1-x}Fe_xO$ samples.

Sample (x)	Particle radius[a] (nm)	Core radius (nm)	Shell thickness (nm)
0.01	16.8	16.2	0.58
0.02	12.6	11.7	0.66
0.03	8.6	8.0	0.62
0.04	7.9	7.3	0.57

[a]Data compiled from Ref. 5.

we used the in-field interaction δM_a plots, each of which is constructed from an initial magnetization curve and the respective ZFC major hysteresis loop.[26] $2\delta M_a(H)$ coincides with the recently defined (and easier to obtain) $\delta M_R(H)$[27] and is practically identical (in both shape and values) to the corresponding classical δM plot constructed from remanence magnetization curves. Figure S2 (see the supplementary material) gives the δM_a plots constructed for the $Cu_{1-x}Fe_xO$ nanoparticles for both $x = 0.02$ and 0.04 using the ZFC magnetization data obtained at 100 K. Weak (given that the amplitude of the δM_a plot is much smaller than the respective saturation magnetization) and negative (demagnetizing-type) interactions are revealed. As expected, these interactions grow stronger with increasing Fe content. We emphasize that the interaction plots do not allow for discrimination between the inter-particle interaction effects and those stemming from intra-particle (e.g., core–shell) coupling.[28]

It was recently shown that the δM_R plots obtained from saturated major hysteresis loops represent a precise measure of the reversal asymmetry in EB systems.[29] We constructed such δM_R^{major} plots (not shown) for both $x = 0.02$ and 0.04 from the magnetization

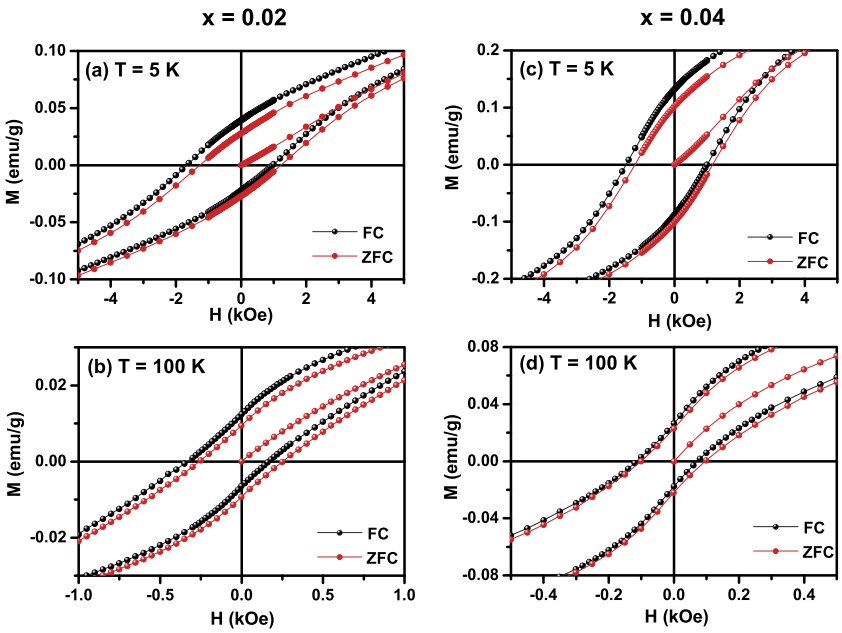

FIG. 6. Magnetic hysteresis loops for the samples $Cu_{0.98}Fe_{0.02}O$ at 5 K (a) and 100 K (b) and $Cu_{0.96}Fe_{0.04}O$ at 5 K (c) and 100 K (d).

TABLE IV. EB and coercivity parameters of the $Cu_{0.98}Fe_{0.02}O$ and $Cu_{0.96}Fe_{0.04}O$ samples.

Sample (x)	H_{EB} (Oe)		H_c (Oe)	
	10 K	100 K	10 K	100 K
0.02	−1335[a]	−249	247	91
0.04	−1318[a]	−94	410	25

[a]Each of these values likely represents a sum of H_{EB} and a field shift due to minor-loop effects.

loops traced at 100 K after FC. These appeared to be essentially nil for all H, meaning that interface exchange coupling does not lead to asymmetric magnetization reversal.

V. CONCLUSIONS

$Cu_{1-x}Fe_xO$ monophasic nanoparticles (with x = 0.02 and 0.04) were synthesized by freeze-drying a mixture of copper and iron acetates followed by heat treatment. These materials are composed of two magnetic phases: a core and a shell. The shell is formed by uncompensated spins (Cu^{2+} and Fe^{3+}), and its thickness (~0.6 nm) is nearly independent of x. It has a SPM behavior at RT, while the core is PM. Upon reducing the temperature, the shell progressively acquires an FM character, while the core freezes to an AFM order. This transition leads to magnetic interactions among neighboring particles and between the core and the shell of each particle. At low temperatures, the $Cu_{1-x}Fe_xO$ nanoparticles presented EB due to the core–shell coupling. The ferromagnetism observed in this system suggests that AFM oxide matrices can be used for diluted magnetic semiconductor applications, if suitably doped.

AUTHORS' CONTRIBUTIONS

All authors contributed equally to this work.

SUPPLEMENTARY MATERIAL

See the supplementary material for more details about the EB analysis.

ACKNOWLEDGMENTS

The authors thank CNPq/Fundação Araucária (Grant No. PRONEX 46824) for the financial support and SQUID-UFSCAR_QD_MPMS3 (Grant No. FAPESP 09/54082-2) for the magnetometry measurements.

DATA AVAILABILITY

The data that support the findings of this study are available from the corresponding author upon reasonable request.

REFERENCES

[1]T. Dietl, H. Ohno, F. Matsukura, J. Cibert, and D. Ferrand, Science **287**, 1019 (2000).
[2]J. M. D. Coey, M. Venkatesan, and C. B. Fitzgerald, Nat. Mater. **4**, 173 (2005).
[3]A. Punnoose, H. Magnone, M. S. Seehra, and J. Bonevich, Phys. Rev. B **64**, 174420 (2001).
[4]G. N. Rao, Y. D. Yao, and J. W. Chen, IEEE Trans. Magn. **41**, 3409 (2005).
[5]A. A. Oliveira, M. I. Valerio-Cuadros, L. F. S. Tupan, F. F. Ivashita, and A. Paesano, Mater. Lett. **229**, 327 (2018).
[6]J. B. Forsyth, P. J. Brown, and B. M. Wanklyn, J. Phys. C: Solid State Phys. **21**, 2917 (1998).
[7]N. M. Basith, J. J. Vijaya, and L. J. Kennedy, Adv. Mater. Res. **938**, 134 (2014).
[8]N. M. Basith, J. J. Vijaya, L. J. Kennedy, and M. Bououdina, Mater. Sci. Semicond. Process. **17**, 110 (2014).
[9]S. Al-Amri, M. Ansari, S. Rafique, M. Aldhahri, S. Rahimuddin, A. Azam, and A. Memic, Curr. Nanosci. **11**, 191 (2014).
[10]S. Layek and H. C. Verma, J. Nanosci. Nanotechnol. **13**, 1848 (2013).
[11]R. A. Borzi, S. J. Stewart, G. Punte, R. C. Mercader, G. A. Curutchet, R. D. Zysler, and M. Tovar, J. Appl. Phys. **87**, 4870 (2000).
[12]H. Yi, G. Xu, H. Cheng, J. Wang, Y. Wan, and H. Chen, Procedia Environ. Sci. **16**, 791 (2012).
[13]S. M. Yakout and A. M. El-Sayed, J. Supercond. Novel Magn. **29**, 2961 (2016).
[14]S. Manna and S. K. De, J. Magn. Magn. Mater. **322**, 2749 (2010).
[15]U. K. Gaur, A. Kumar, and G. D. Varma, J. Mater. Chem. C **3**, 4297 (2015).
[16]S. J. Stewart, R. A. Borzi, G. Punte, and R. C. Mercader, Phys. Rev. B **57**, 4983 (1998).
[17]A. A. Oliveira, M. I. Valerio-Cuadros, L. F. S. Tupan, F. F. Ivashita, and A. Paesano, Jr., Hyperfine Interact. **240**, 53 (2019).
[18]M. Bandyopadhyay and S. Dattagupta, Phys. Rev. B **74**, 214410 (2006).
[19]S. Bedanta and W. Kleemann, J. Phys. D: Appl. Phys. **42**, 013001 (2009).
[20]A. K. Pramanik and A. Banerjee, Phys. Rev. B **82**, 094402 (2010).
[21]Y. R. Park, K. J. Kim, S.-l. Choi, J. H. Lee, H. J. Lee, C. S. Kim, and J. Y. Park, Phys. Status Solidi Basic Res. **244**, 4578 (2007).
[22]O. Petracic, Superlattices Microstruct. **47**, 569 (2010).
[23]J. Fock, M. F. Hansen, C. Frandsen, and S. Mørup, J. Magn. Magn. Mater. **445**, 11 (2018).
[24]I. V. Goldanskii and R. H. Herber, *Chemical Applications of Mössbauer Spectroscopy*, edited by V. I. Goldanskii and R. H. Herber (Academic Press, New York, 1968).
[25]A. Harres, M. Mikhov, V. Skumryev, A. M. H. de Andrade, J. E. Schmidt, and J. Geshev, J. Magn. Magn. Mater. **402**, 76 (2016).
[26]V. Masheva, J. Geshev, and M. Mikhov, J. Magn. Magn. Mater. **137**, 350 (1994).
[27]J. Geshev, J. Magn. Magn. Mater. **467**, 135 (2018).
[28]J. A. De Toro, M. Vasilakaki, S. S. Lee, M. S. Andersson, P. S. Normile, N. Yaacoub, P. Murray, E. H. Sánchez, P. Muñiz, D. Peddis, R. Mathieu, K. Liu, J. Geshev, K. N. Trohidou, and J. Nogués, Chem. Mater. **29**, 8258 (2017).
[29]J. Geshev, L. L. Bianchi, R. F. Lopes, J. L. Salazar Cuaila, and A. Harres, J. Magn. Magn. Mater. **497**, 166061 (2020).